Calibration of an adaptive microscope using phase diversity

Delphine Débarre, Thibault Vieille, Aurélie Facomprez, Pierre Mahou, and Emmanuel Beaurepaire

Laboratory for Optics and Biosciences, Ecole Polytechnique ParisTech, CNRS, and INSERM, 91128 Palaiseau, France

ABSTRACT

Accurate control over the phase and amplitude modulation in an adaptive microscope is essential to the quality of aberration correction that can be achieved. In this paper we present a robust and compact method for characterising such amplitude and phase modulation in the pupil plane of the focussing objective. This method, based on phase diversity, permits calibrating the microscope as a whole and thus avoids errors in the alignment of the wavefront shaping device after calibration and the resulting imprecision in the induced modulation: by acquiring three 2D images of the point spread function at different distances from the focal plane, we show that the electric field distribution at the pupil plane can be retrieved using an iterative algorithm. We have applied this technique to the characterisation of the phase modulation induced by a deformable mirror when conjugated with the entrance pupil of different objectives, which permits accurate evaluation of the performance of the mirror for subsequent aberration correction.

Keywords: Adaptive optics, aberration correction, deformable mirror, phase diversity, microscopy

1. INTRODUCTION

Over the past decade, aberration correction schemes for microscopy have been developed to restore the quality of images acquired deep within aberrating samples. The aim of such schemes is to compensate for the optical aberrations introduced by the optical system and the sample by applying an opposite deformation to the wavefront using a deformable mirror (DM) or a spatial light modulator (SLM).[1] Such techniques have proven particularly useful for nonlinear microscopies, which are often used for imaging thick, complex biological samples.[2,3]

When setting up aberration correction in an existing microscope, the active element should be inserted in the optical setup and the adaptive microscope should be calibrated for accurate control of the shaped wavefront. However, it is often impractical and expensive to also incorporate a wavefront sensor such as a Shack-Hartmann sensor, in particular when image-based correction approaches are used that do not employ a wavefront sensor.[1,4–6] As an alternative, we have developed a calibration scheme of an adaptive microscope based on electric field retrieval from measurements of the microscope point spread function (PSF). This method provides precise and simple *in situ* calibration of the modulation of the excitation electric field at the entrance pupil of the focussing objective with minimal change in the optical setup. In the following, we will restrict ourselves to the case of nonlinear microscopy, for which only the excitation wavefront distortion is compensated, but our results can be extended to the calibration of the emission wavefront, e.g. for the case of confocal microscopy.

In this paper, we will first analyse the effect of calibration errors in the setup on the aberration effectively introduced by the mirror (Section 3). We will then introduce our calibration method (Section 4) and present experimental results (Section 5). Finally, using calibration data, we will analyse the properties of our deformable mirror for aberration correction in a nonlinear microscope (Section 6).

Further author information: Send correspondence to D.D.
E-mail: delphine.debarre@polytechnique.edu, Telephone: +33 (0)1 69 33 50 21
www.lob.polytechnique.fr

Three-Dimensional and Multidimensional Microscopy: Image Acquisition and Processing XIX, edited by Jose-Angel Conchello, Carol J. Cogswell, Tony Wilson, Thomas G. Brown, Proc. of SPIE Vol. 8227, 822708 · © 2012 SPIE · CCC code: 1605-7422/12/$18 · doi: 10.1117/12.908632

2. IMPACT OF CALIBRATION ERRORS ON THE CONTROL OF THE WAVEFRONT

In most implementations of adaptive optics for microscopy, the wavefront shaping device is a deformable mirror: compared to a SLM, this type of device offers a better power efficiency (typically 90-95% reflectivity) independently of the incident polarisation and a smaller response time. DMs should however be carefully calibrated before use as the relationship between the vector of command voltages sent to the actuators of the mirror and the resulting phase modulation is not straightforward. Moreover, this calibration depends strongly on the exact location of the DM within the microscope, the magnification between the DM and the focussing objective, and the pupil size of the chosen objective: indeed, in the common case where the DM is conjugated with the entrance pupil of the objective (thereby inducing a constant phase modulation over the whole field of view) these factors determine the region of the DM that is imaged on this entrance pupil, and hence over which the desired wavefront should effectively be created. If the size or the position of this region on the DM surface are estimated with a small error, this leads to an error in the applied phase that is usually unknown and might deteriorate the quality of subsequent aberration correction.

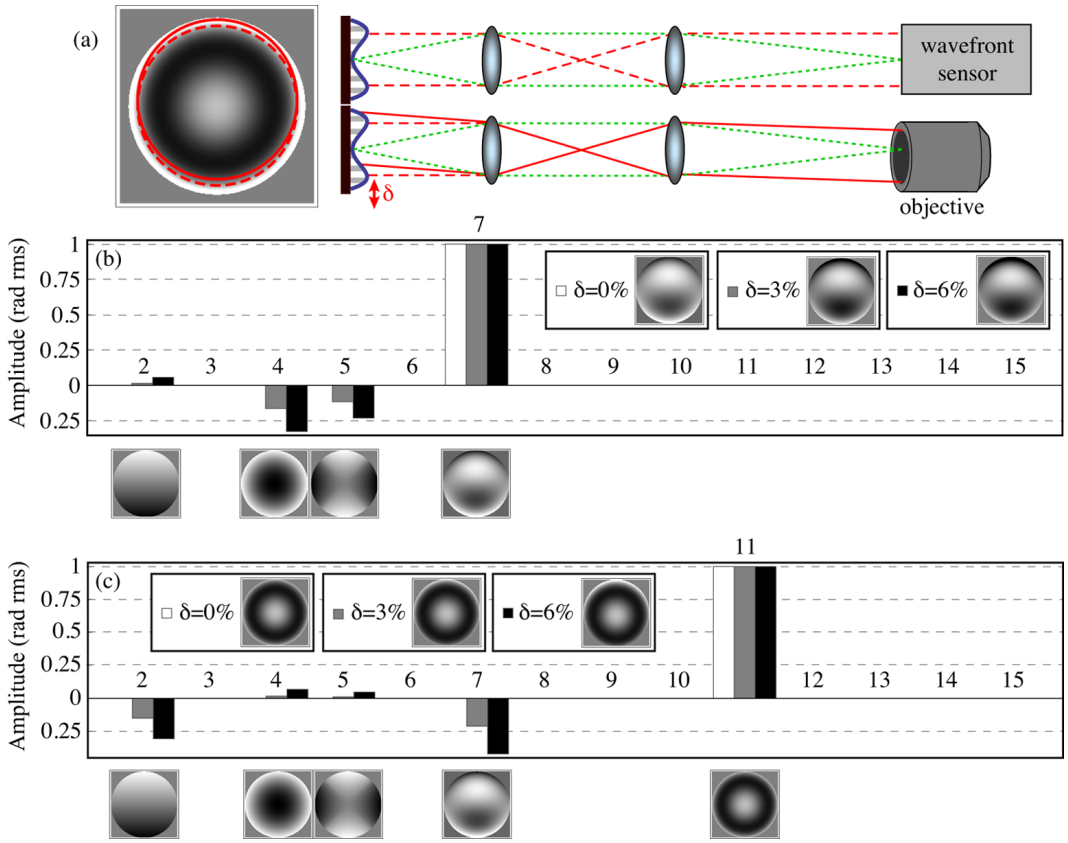

Figure 1. (a), example of imprecise DM calibration: measurement of the phase modulation by the DM was performed using a wavefront sensor placed at the approximate location of the objective, but with a small lateral position error δ. Plane/dashed red lines, light path; the DM is conjugated with the entrance pupil of the objective (dotted lines). (b), resulting aberration introduced in the entrance pupil of the microscope when applying the command to create coma (z=7) over the calibrated region. (c), resulting aberration when trying to introduce spherical aberration (z=11).

This effect is illustrated in figure 1 in the case of a small offset error, in the case of two commonly used Zernike modes: coma (z=7, see Appendix A) and spherical aberration (z=11). Here we modelled the case where the mirror was calibrated over a region of the right size using previous knowledge of the pupil size of the objective and the magnification factor between the objective and the DM; but assuming that this region should be centred

on the DM, which was not perfectly realised due to a slight alignment error δ (figure1, (a)). The phase created over a disk corresponding to the image of the objective is plotted as a function of δ and decomposed over Zernike modes defined on this correct region (figure1, (b) and (c)). Even for an error as small as 3% of the pupil size, the amplitude of aberration in unwanted modes reaches up to 20% of the amplitude in the desired mode. For a DM of a few mm in diameter, this only corresponds to an error in the lateral positioning of the device of a few hundreds of microns, a precision that is difficult to achieve in practice.

Similar error is obtained when calibrating the DM using an erroneous estimate of the pupil size, as illustrated on figure 2. This is a common situation since the exact size of the entrance pupil is often unknown. The effect of the change of the support size for Zernike polynomials has been described with more details e.g. in[7] .

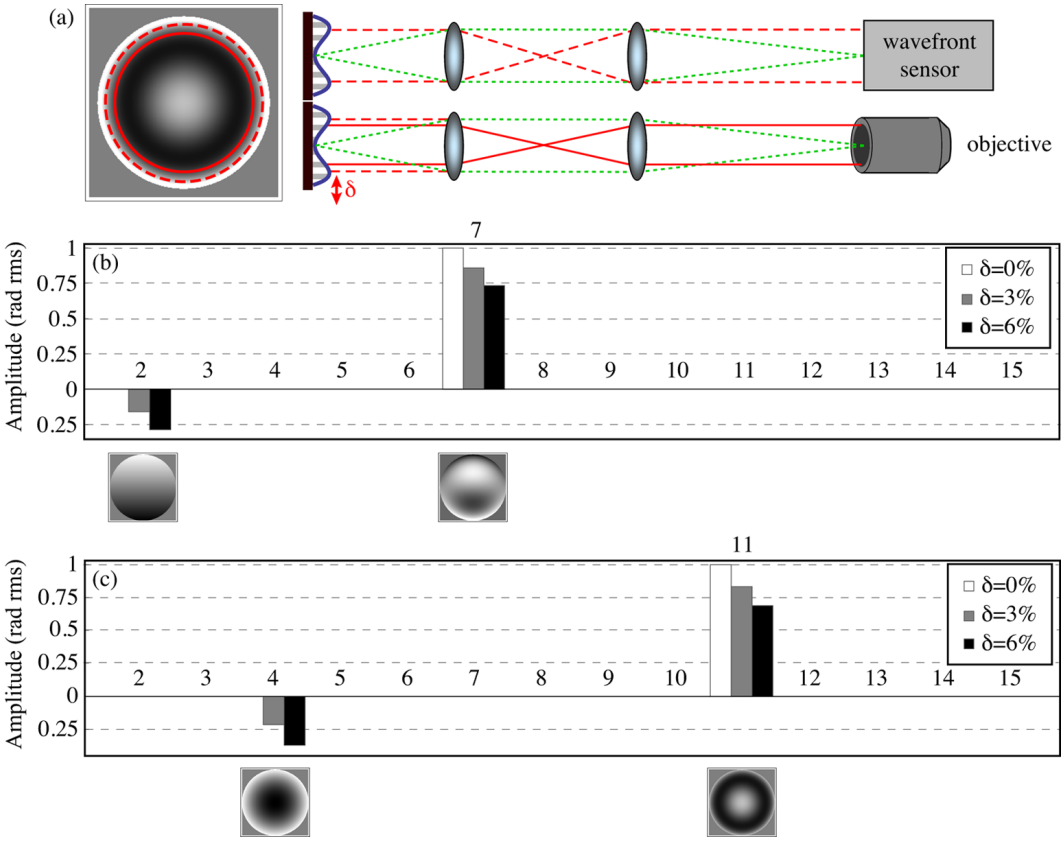

Figure 2. (a), example of imprecise DM calibration: measurement of the phase modulation by the DM was performed assuming a pupil size for the objective slightly larger than the real one. Plane/dashed red lines, light path; the DM is conjugated with the entrance pupil of the objective (dotted lines). (b), resulting aberration introduced in the entrance pupil of the microscope when applying the command to create coma (z=7) over the calibrated region. (c), resulting aberration when trying to introduce spherical aberration (z=11).

Such calibration errors have a dramatic effect on aberration correction when a sensorless aberration scheme is used: in such approaches, the phase is not measured directly, so that the estimation of the corrected phase only relies on the previous calibration of the mirror. Since errors appear even for small changes in position of the DM or in pupil size of the objective, it is difficult to avoid them entirely when calibrating the DM without taking into account the whole optical setup.

3. CALIBRATION OF AN ADAPTIVE MICROSCOPE

3.1 Methods for calibration

In order to avoid such calibration mistakes, the DM should not be calibrated over the estimated size of the objective pupil, but rather by also taking into account the other elements in the microscope: the adaptive microscope should be calibrated as a whole, so as to measure the phase and/or amplitude modulation at the entrance pupil of the objective (and hence at the focal point).

In figure 3, we propose three possible schemes to perform this calibration with good precision. Although the phase measurement method vary, they all rely on the use of a mirror located in the focal plane of the focussing objective and a beamsplitter plate used to separate a part of the back-reflected light and to send it to a detector.

- The first configuration (figure 3, (a)) corresponds to interferometric measurement of the phase: the fraction of the incoming light modulated by the DM is combined with the unmodulated fraction to generate fringes of equal thickness which are imaged on a CCD camera after passing through the objective. The phase difference between the two paths is then inferred from the fringe pattern as described in[8] .
- The second configuration uses a direct wavefront sensor such as a Shack-Hartmann sensor or a lateral shearing interferometer. The sensor is conjugated with the entrance pupil of the objective.
- Finally, in the third configuration, 2D images of the system point spread function (PSF) can be acquired on a CCD camera in three planes in the vicinity of the focal plane, and the electric field at the exit of the objective is reconstructed using a phase retrieval algorithm.

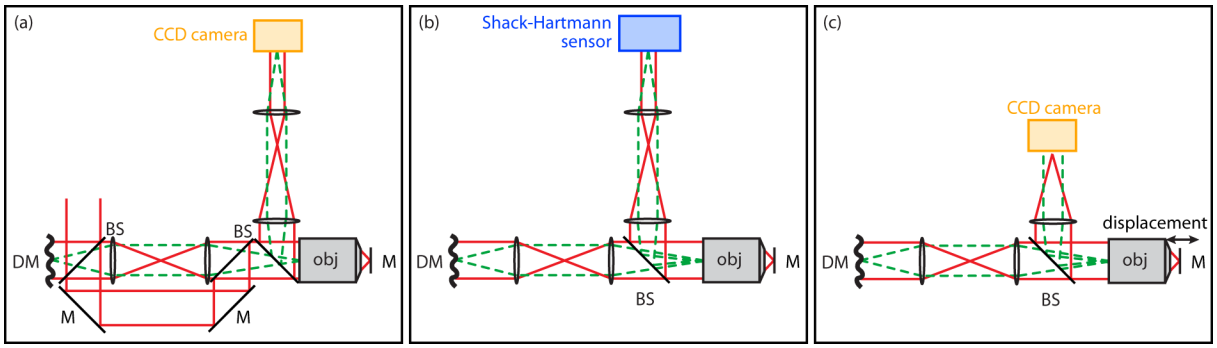

Figure 3. Methods for precise calibration of an adaptive microscope. (a), interferometric phase measurement; (b), direct wavefront sensing using e.g. a Shack-Hartmann sensor; (c), electric field retrieval using phase diversity. BS, beam splitter; M, mirror; obj; objective. Plain line, light path; the dashed lines show the conjugated planes in the optical setup.

The first method is efficient and relatively simple to set up, but requires space to built the interferometer, and can only be used with temporally coherent light, thereby excluding pulsed light sources such as used in nonlinear microscopy. The second option is relatively straightforward, but requires a wavefront sensor. In case this sensor is not further used for aberration correction, this makes the calibration process unnecessarily expensive. Furthermore, both these two first methods require that the magnification between the objective pupil and the detector be adjusted depending on the objective to be calibrated.

Alternatively, phase retrieval from PSF images can be used to measure both the phase and the amplitude modulation in the pupil plane of the objective. This method is cost-effective, more compact than the first two and offers greater flexibility: indeed, calibration can be performed with most objectives without changing the calibration arm. In the following, we will detail the principles of this calibration technique.

3.2 PSF measurements

The PSF are measured as described in[9] : a mirror M located at an axial distance $z = z_0$ from the focal plane of the objective (figure 3(c)) reflects the incident light towards a 50/50 beamsplitter. The light reflected by the beamsplitter is then focussed onto a CCD camera to form a magnified image of the 2D PSF at position $z = 2z_0$. This image may be distorted by aberrations on the path between the mirror and the CCD, so that the imaged PSF can be expressed as the Fourier transform of a modified pupil function:

$$\Pi_{tot}(\vec{r}) = \Pi_{ill}(\vec{r})T_o(\vec{r})T_d(-\vec{r})e^{j(\phi_o(\vec{r})+\phi_d(-\vec{r})+\Delta\phi(\vec{r},z_0))}, \quad (1)$$

where Π_{ill} is the illumination pupil function, T_o and ϕ_o (respectively T_d and ϕ_d) are the objective (resp. detection path) amplitude transmission and aberration phase, $\vec{r}$ is the normalised pupil plane coordinate, and $\Delta\phi(\vec{r}, z_0)$ is the defocus term given by :

$$\Delta\phi(\vec{r}, z_0) = 2knz_0\sqrt{1-(NA/n)^2r^2}, \quad (2)$$

where k is the wave vector in vacuum, n is the refractive index of the immersion medium and NA is the numerical aperture of the objective. This modified pupil function differs from the pupil function of the microscope (which, by Fourier Transform, yields the microscope PSF) by a multiplicative term $T_d(-\vec{r})e^{j\phi_d(-\vec{r})}$: hence we do not strictly measure the microscope PSF. However since this multiplicative function is constant, it does not prevent retrieving the pupil function modulation due to the DM and thus calibrating it.

3.3 Electric field retrieval

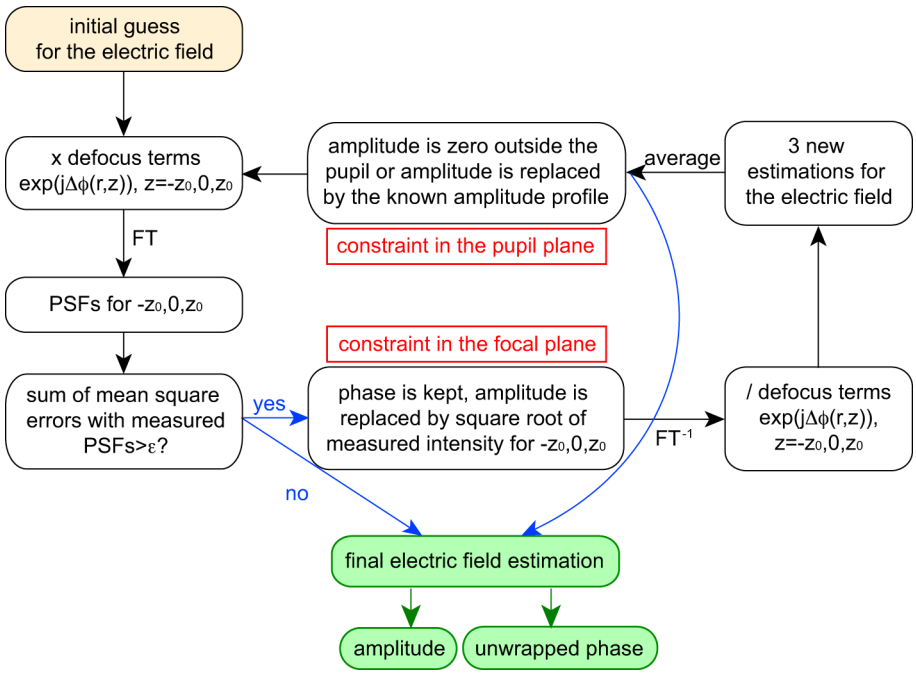

Figure 4. Flow diagram of the electric field retrieval algorithm. See[10] for more details and typical values of the various parameters. Our phase retrieval software (written in LabView) can be downloaded at[11] .

Using 3 PSF measurements acquired at different z_0 positions, this modified pupil function $\Pi_{tot}(\vec{r})$ was then calculated by use of a modified Gershberg-Saxton algorithm taking into account the large numerical aperture of usual objective lenses. The algorithm is similar to the one described in[12] . However, since the PSF was measured using reflected light rather than fluorescence from a small bead around the focus, raw images exhibited high

signal-to-noise ratio, which permitted the use of only three PSF images taken at positions z_0, 0 and $-z_0$, instead of four in[12] . This also removed the need for pre-filtering of the data and filtering of the retrieved phase between iterations of the phase retrieval algorithm. Finally, no deconvolution step was required to remove the influence of the finite size of the beam.

The algorithm is presented in more details in[10] . Briefly, the guess for $\Pi_{tot}(\vec{r})$ at iteration i was used to calculate three 2D amplitude PSFs corresponding to positions z_0, 0 and $-z_0$. These reconstructions were compared to the measured intensity images to estimate the quality of the pupil function guess: if ϵ, the sum of the mean square differences between each reconstructed intensity profile (obtained as the squared absolute value of the reconstructed amplitude PSF) and the corresponding measured profile, normalised to the sum of the mean square values of the three measured intensity profiles, was smaller than 0.1%, or if the relative variation of ϵ between iterations i-1 and i was smaller than 0.1%, the iterative loop was terminated and $\Pi_{tot}(\vec{r})$ at iteration i was used to calculate the estimate of the amplitude and phase of the electric field. Otherwise, the phase of the reconstructions were kept while their amplitude were replaced by the measured profiles. After an inverse Fourier transform and removal of the defocus term, the new guess at iteration i+1 for $\Pi_{tot}(\vec{r})$ was calculated by averaging the three estimates for z_0, 0 and $-z_0$ and applying an appropriate constraint on the resulting amplitude: either the intensity is simply set to zero outside of the back aperture of the objective and no further assumption is made on the amplitude profile within the pupil; or, if the intensity profile is already known (e.g. from a previous measurement when phase-only modulation is applied), the calculated profile is replaced by the readily known profile. Finally, phase unwrapping was performed as described in[8] .

A flow diagram of the algorithm is shown on figure 4. The in-house developed software for electric field retrieval using this algorithm is available for download from our website[11] .

Measured 2D PSFs along with the reconstructed amplitude and phase profiles are presented on figure 5, on the example of the calibration of phase-only modulation of a DM conjugated with the microscope objective. These data illustrate the robustness of our retrieval process, which permits retrieving the phase with good accuracy even in regions with small electric field amplitude (e.g. the edge of the objective pupil).

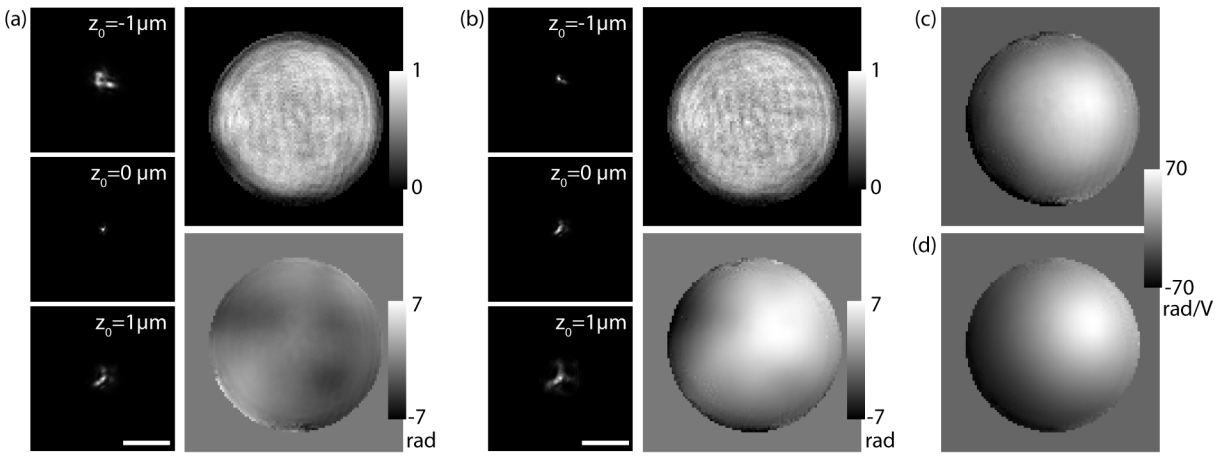

Figure 5. Calibration of the phase-only modulation induced by one actuator of our DM conjugated with a 60x, 1.2NA, water immersion objective (Olympus). (a), PSF images (left) and retrieved amplitude (right, top) and phase (right, bottom) in the pupil plane of the objective, for a voltage set to zero applied to all of the actuators. The amplitude lookup table is scaled arbitrarily. Scale bar, 10μm. (b), PSF images (left) and retrieved amplitude (right, top) and phase (right, bottom) in the pupil plane of the objective, for a voltage set to zero applied to all of the actuators but one. The amplitude lookup table is scaled arbitrarily. Scale bar, 10μm. (c), phase modulation obtained from the phase profiles in (a) and (b). (d), the signal-to-noise ratio of the phase modulation profile is significantly increased when fitting several such retrieved phase profiles. Here, 20 profiles obtained for different voltages applied to the same actuator were used. (c) and (d) share the same colour scale.

This calibration method is similar to that developed by Turaga et al.[13] . In their implementation, a single PSF image is acquired for each voltage sent to the actuator, and the phase modulation induced by the mirror

is used instead of defocus to obtained the phase diversity required for phase retrieval. However, this scheme is limited to phase retrieval as the intensity profile has to be set arbitrarily before phase retrieval. Furthermore, the retrieval algorithm is much more complex in this case.

Here, we took advantage from the fact that most microscopes have a motorised focussing device, either by movement of the sample stage or of the objective. Furthermore, since in most cases an imaging port of the microscope can be used to install the camera, with the beamsplitter replacing the usual dichroic beamsplitter separating the excitation light and the signal, our scheme can be installed on most microscopes with little, if any, modification of the existing experimental setup.

4. ADAPTIVE MICROSCOPE CHARACTERIZATION

One of the benefits of our scheme is that it can be used to characterise the properties of an adaptive microscope for several objectives with different magnifications and numerical apertures, without modification of the measuring scheme[10] . Here we illustrate this property on the example of two different objectives: a 25x, 1.05NA and a 60x, 1.2NA objective (Olympus). Both objectives are water immersion and coverslip corrected. The DM used here is a MIRAO-52e with 52 actuators (Imagine Optics, France). The magnification was set so that the pupil of the 25x objective was slightly underfilled by the image of the DM, resulting in an effective NA of 0.95. Therefore the whole DM surface was transmitted through the objective. On the contrary, since the entrance pupil diameter of the 60x objective is much smaller than that of the 25x objective, only a smaller number of actuators influences the pupil phase modulation.

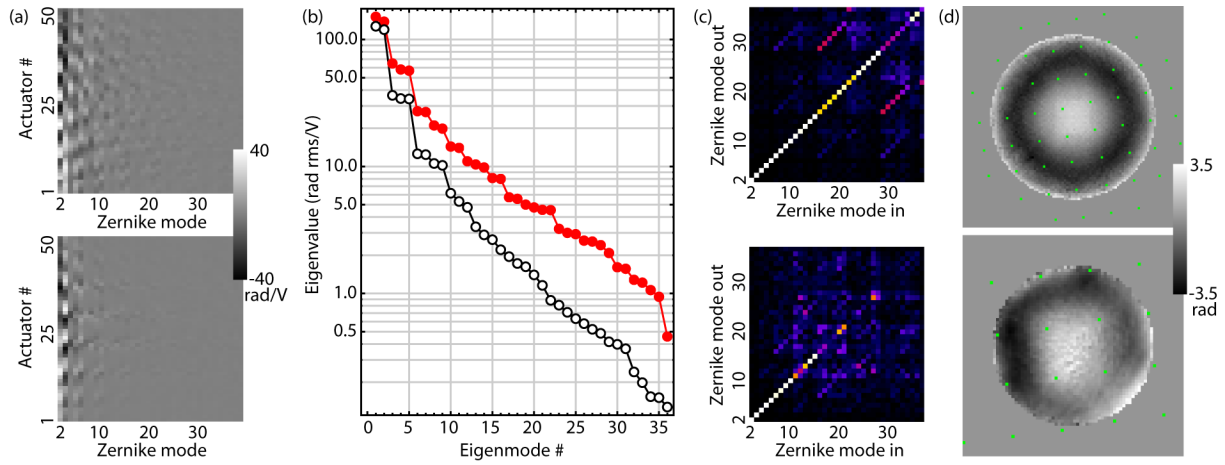

Figure 6. Calibration of our adaptive microscope with phase-only modulation using two different objectives. (a), Zernike mode amount induced by each actuator for a unit voltage applied, with the 25x (top) and 60x (bottom) objectives; (b), eigenvalues for the eigenmodes calculated by singular value decomposition of (a). Red dots, 25x, objective; Black circles, 60x objective. (c), similarity matrix; and (d), measured phase modulation when applying the command for first order spherical aberration. Top, 25x objective; bottom, 60x objective. Green dots, approximative location of the actuators of the DM.

This is illustrated on figure 6: in (a), the amount of each Zernike mode created when a voltage is applied to a given actuator. As expected, the amplitude of higher order modes created in the case of the 25x objective (top) is much larger than for the 60x objective (bottom). As a result, when considering the eigenmodes of the system projected onto Zernike modes (b), the number of significant eigenvalues is much larger for the 25x (red dots) than for the 60x objective (black circles). These eigenmodes are obtained from the matrices in (a) by singular value decomposition, as described in[8] .

In order to produce Zernike modes in the entrance pupil of the objective, a pseudo-inversion of the matrices in (a) is realised using only eigenmodes in (b) that have eigenvalues greater than a chosen threshold, chosen so as to minimise the amplification of the noise in the measurement, and to avoid saturation of the DM[8] . Here we experimentally set this threshold to 2 rad/V, so that 29 eigenmodes were used for the 25x objective, versus

16 for the 60x objective. The resulting modes are characterised by the similarity matrix **M**, defined as the product of the matrices in (a) times their pseudo-inverse. **M** is plotted in (c) for both objectives, and shows the combination of Zernike modes produced when sending the vector of command calculated to produce one chosen mode. As expected, the number of modes that can be accurately produced is greatly reduced in the case of the 60x objective.

This is directly linked to the number of actuators that are imaged in the objective pupil, as represented in (d). The phase shown in (d) is the phase modulation induced by the vector of command calculated to induce one radian rms first order spherical aberration. In the case of the 25x objective, the phase is accurately produced, whereas the result for the 60x objective poorly resembles spherical aberration due to the small number of actuators imaged within the pupil. This shows that such a DM, with a reduced number of actuators and slowly spatially varying influence functions (figure 5(d)), has limited versatility in terms of the objectives that can be used without changing the optical magnification between the DM and the objective. This is greatly improved when using a DM with a greater number of actuators.

5. CONCLUSION

In this paper we have presented a method for characterising the amplitude and phase modulation properties of an adaptive microscope in the pupil plane of the focussing objective. This method, based on phase diversity, permits calibrating the microscope as a whole and thus avoids errors in the positioning of the readily calibrated DM, and the resulting imprecision in the induced modulation. We have applied this technique to the characterisation of the phase modulation induced by our deformable mirror when conjugated with the entrance pupil of two different objectives, which permits accurate evaluation of the performance of the mirror and subsequent aberration correction.

ACKNOWLEDGMENTS

This work was supported by the Agence Nationale de la Recherche (RIB2007 program). The authors thank Jerome Mertz for fruitful discussions.

APPENDIX A. ZERNIKE MODES NUMBERING SCHEME

Table 1. Zernike modes 1 to 15 and numbering scheme. The modes are expressed over the unit disk as functions of r and θ with $0 < r < 1$ and $0 < \theta < 2\pi$.

Index, z	Zernike mode	Name
1	1	Piston
2	$2r\cos\theta$	Tip
3	$2r\sin\theta$	Tilt
4	$\sqrt{3}(2r^2-1)$	Defocus
5	$\sqrt{6}r^2\cos 2\theta$	Astigmatism, 1st order
6	$\sqrt{6}r^2\sin 2\theta$	Astigmatism, 1st order
7	$2\sqrt{2}(3r^3-2r)\cos\theta$	Coma
8	$2\sqrt{2}(3r^3-2r)\sin\theta$	Coma
9	$2\sqrt{2}r^3\cos 3\theta$	Trefoil
10	$2\sqrt{2}r^3\sin 3\theta$	Trefoil
11	$\sqrt{5}(6r^4-6r^2+1)$	Spherical aberration
12	$\sqrt{10}(4r^4-3r^2)\cos 2\theta$	Astigmatism, 2nd order
13	$\sqrt{10}(4r^4-3r^2)\sin 2\theta$	Astigmatism, 2nd order
14	$\sqrt{10}r^4\cos 4\theta$	tetrafoil
15	$\sqrt{10}r^4\sin 4\theta$	tetrafoil

REFERENCES

[1] Booth, M., Neil, M., Juskaitis, R., and Wilson, T., "Adaptive aberration correction in a confocal microscope," *P. Natl. Acad. Sci. USA* **99**(9), 5788–5792 (2002).

[2] Rueckel, M., Mack-Bucher, J. A., and Denk, W., "Adaptive wavefront correction in two-photon microscopy using coherence-gated wavefront sensing," *P. Natl. Acad. Sci. USA* **103**(46), 17137–17142 (2006).

[3] Olivier, N., Débarre, D., and Beaurepaire, E., "Dynamic aberration correction for multiharmonic microscopy," *Opt. Lett.* **34**(20), 3145–3147 (2009).

[4] Marsh, P., Burns, D., and Girkin, J., "Practical implementation of adaptive optics in multiphoton microscopy," *Opt. Express* **11**(10), 1123–1130 (2003).

[5] Débarre, D., Botcherby, E. J., Booth, M. J., and Wilson, T., "Adaptive optics for structured illumination microscopy," *Opt. Express* **16**, 9290–9305 (2008).

[6] Débarre, D., Botcherby, E. J., Watanabe, T., Srinivas, S., Booth, M. J., and Wilson, T., "Image-based adaptive optics for two-photon microscopy," *Opt. Lett.* **34**(16), 2495–7 (2009).

[7] Lundstrom, L. and Unsbo, P., "Transformation of zernike coefficients: scaled, translated, and rotated wavefronts with circular and elliptical pupils," *J Opt Soc Am A* **24**(3), 569–577 (2007).

[8] Booth, M., Wilson, T., Sun, H., Ota, T., and Kawata, S., "Methods for the characterization of deformable membrane mirrors," *Appl. Opt.* **44**(24), 5131–5139 (2005).

[9] Botcherby, E., Juskaitis, R., Booth, M., and Wilson, T., "An optical technique for remote focusing in microscopy," *Opt. Commun.* **281**(4), 880–887 (2008).

[10] Débarre, D., Vieille, T., and Beaurepaire, E., "Simple characterisation of a deformable mirror inside a high numerical aperture microscope using phase diversity," *J. Microsc.* **244**, 136–143 (2011).

[11] Software for phase retrieval from PSF images available at: http://www.lob.polytechnique.fr/home/research/advanced-microscopies-and-tissue-physiology/wavefront-engineering-for-nonlinear-microscopy-23339.kjsp?RH=1257431537245.
[12] Hanser, B., Gustafsson, M., Agard, D., and Sedat, J., "Phase retrieval for high-numerical-aperture optical systems," *Opt. Lett.* **28**(10), 801–803 (2003).
[13] Turaga, D. and Holy, T. E., "Image-based calibration of a deformable mirror in wide-field microscopy," *Appl. Opt.* **49**(11), 2030–2040 (2010).